ORTEC®

AN61
Application Note

How Counting Statistics and the ADC Sampling Interval Control Mass Accuracy in Time-of-Flight Mass Spectrometry

D. A. Gedcke

Summary

Compared to a Time-to-Digital Converter*, a Digital Signal Averager enables several orders of magnitude higher ion rates to be processed in a time-of-flight mass spectrometer. A Time-to-Digital Converter is limited by a ceiling on the acceptable ion rate, because it can respond only to single-ion pulses1. A Digital Signal Averager, on the other hand, can respond linearly to any number of ions in each pulse, because it employs an ADC to sample the signal. This difference in performance is important, because mass accuracy, isotope ratio accuracy, and detection limits are inversely proportional to the square root of the number of ions counted in a peak. More ions yield better accuracy and lower detection limits.

This application note develops the formulae defining the dependence of mass accuracy and peak area uncertainty on a) ion counting statistics and b) the sampling interval of the ADC in the Digital Signal Averager. For normal operating conditions, the systematic error from the sampling interval is negligible relative to the random error from ion counting statistics. Consequently, interleaved 2-GS/s sampling with a single 500-MS/s ADC yields the same statistical precision as 2-GS/s sampling with 4 parallel 500-MS/s ADCs. But, the former method is significantly more cost-effective.

The Time-of-Flight Mass Spectrometer

Figure 1 illustrates the application of a Digital Signal Averager in an orthogonal-acceleration time-of-flight mass spectrometer (TOF-MS). Ionized molecules from the source are injected into the acceleration region of the mass spectrometer at a 90° angle to the axis of the field-free drift tube. Typically, the ionized molecules are produced from a sample that contains a mixture of molecules having different masses. The function of the mass spectrometer is to separate the molecules according to mass, accurately measure the mass, and determine the relative concentrations of the molecules of each mass. This is accomplished by accelerating the ionized molecules with a voltage pulse of amplitude V applied to the acceleration plate. Subsequently, the differences in flight times of the ions from the acceleration region to the detector at the other end of the drift tube are measured. The flight time, t, from the grounded grid of the acceleration region to the detector is related to the mass, m, of the ionized molecule by equation (1).

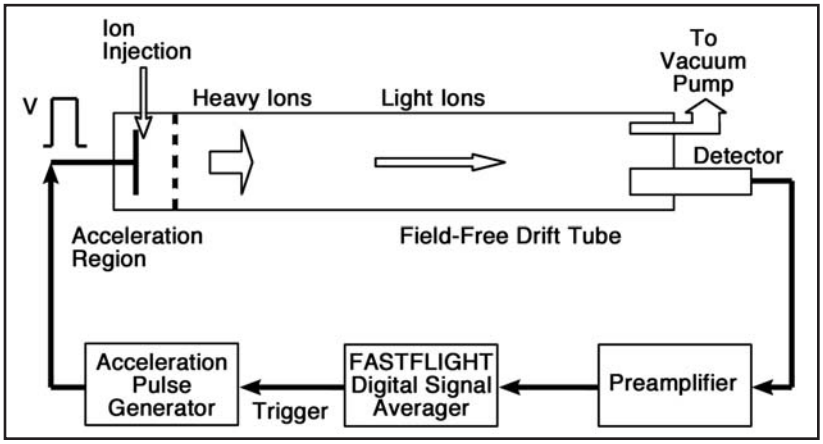

Figure 1. A simplified representation of an orthogonal-acceleration time-of-flight mass spectrometer with a digital signal averager acquiring the spectra.

$$t^2 = \left[\frac{d^2}{2V}\right]\left(\frac{m}{z}\right) \qquad (1)$$

where d is the length of the flight path from grounded grid to detector, and z is the charge on the ionized molecule. Obviously, molecules with lower values of m/z will have shorter flight times than molecules with higher values of m/z. When molecules of a specific m/z value arrive at the detector, the detector responds by producing an output pulse of a few nanoseconds duration and with an amplitude that is nominally proportional to the number of molecules that strike the detector. The preamplifier amplifies this signal and presents it to the analog input of the digital signal averager.

*A time-to-digital converter (TDC) is also known as a time digitizer.

The operation of the digital signal averager is depicted in Figure 2. The analog signal from the detector and preamplifier is fed to the input of an 8-bit sampling ADC. At regular intervals of T_s seconds, a sampling clock commands the ADC to take a brief sample of the analog input signal. The ADC converts this sample to a digital number proportional to the analog signal amplitude. The result is a stream of digital numbers flowing into the Summing Memory. This stream of numbers is a digital representation of the varying analog signal presented to the ADC input.

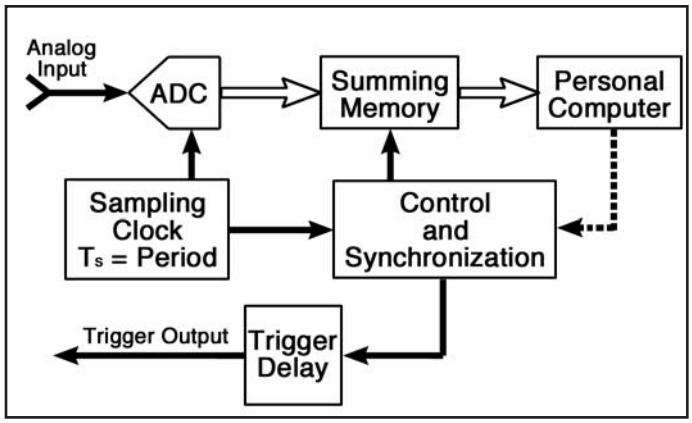

Figure 2. A simplified schematic of the FASTFLIGHT Digital Signal Averager.

To maintain good stability, the ADC never stops sampling. Consequently, some means of synchronization with the acceleration pulse in the TOF-MS is required. The Control and Synchronization block performs that function. When the digital signal averager is ready to record a single scan of the flight times, the Control and Synchronization block sends a Trigger Output pulse to the Acceleration Pulse Generator in the TOF-MS. The leading edge of the Trigger Output pulse is precisely synchronized with a sampling command to the ADC. At the same time, the Summing Memory is told to start recording the stream of digital numbers from the ADC. This scan continues until the slowest ions have been detected. At the end of the scan the Summing Memory contains a digital record of the detector output signal as illustrated in Figure 3.

Because the resolving power is circa 7,000:1, the peaks corresponding to a specific m/z value appear to be narrow lines sitting on a flat background in Figure 3a. Each of these lines is typically composed of several peaks, as illustrated in Figure 3b by the magnified view of the line at 50,000 ns from Figure 3a. The dots in Figure 3b correspond to the ADC samples.

For a single scan, the number of ions counted in the smaller peaks is very low. As a result, the peaks are imprecisely defined, and the detection limits are high. To solve this problem, the scan is repeated a large number of times, with the results of each scan being added to the sum of the previous scans. If the scan length is 100 ms, 1000 scans can be implemented and summed in 0.1 seconds. This improves the precision and detection limits in proportion to the square root of the number of scans. If the data from the sum of a large number of scans is divided by the number of scans, the result is the average signal for one scan. This is why the instrument is called a signal averager.

At the end of the summing process, the resulting spectrum is transferred to the supporting computer for storage on a hard disk, while the next sum is being acquired. Because the digital signal averager performs the summing rapidly in its hardware memory, it can keep up with the fast data flow required to support a chromatograph as the source of the molecules. A chromatograph typically requires the TOF-MS to record summed spectra at 0.1-second intervals for as long as 30 minutes. Although the spectra are naturally acquired with flight time defining the x axis, equation (1) can be used to calibrate the horizontal axis in terms of m/z.

How the Sampling Interval Affects Mass Accuracy

As depicted in Figure 3b, the shape of a peak in the time-of-flight spectrum is approximately Gaussian. The mathematical model for a Gaussian peak is expressed by equation (2):

$$V(t) = \frac{A}{\sqrt{2\,\pi\,\sigma^2}}\, e^{-(1-T)^2 / 2\,\sigma^2} \qquad (2)$$

where A is the area of the peak, T is the centroid of the peak, and σ is the standard deviation of the peak. For a Gaussian peak, the Full Width at Half Maximum height (FWHM) is related to s by

$$FWHM = 2\sqrt{2\,ln(2)}\;\; \sigma = 2.35\,\sigma \qquad (3)$$

The key question is, "How small a sampling interval is required to determine the position of the Gaussian peak to the desired accuracy?" A simple way to study this issue is to use all the samples across the peak to determine its centroid, or first moment. In other words, the centroid is computed from the discrete samples by equation (4):

$$T_C = \frac{\sum_i V_i\, t_i}{\sum_i V_i} \qquad (4)$$

where t_c is the centroid or first moment of the sampled peak, t_i is the time coordinate of the i^{th} sample on the peak, and V_i is the voltage amplitude measured at the i^{th} sample.

At issue is the systematic error between the result for t_c from equation (4) and the true value, T, for the centroid in equation (2). Two simple examples clarify the source of the systematic error. Consider a Gaussian peak on which only two, widely-spaced samples have been taken. If the two samples are exactly symmetrically located with respect to the centroid of the peak, the answer from equation (4) will exactly match the value of T from equation (2). However, if the samples are asymmetrically located relative to the true centroid, equation (4) will yield an answer with a systematic error. Now consider 3, widely-spaced samples on that same peak, with equal distances between the central point and the two outside points. If the central point lies exactly on the centroid of the peak, the answer from equation (4) yields the correct value for T. But, if the central point is shifted away from the centroid, a systematic error will result from equation (4). When multiple points span the peak, these two examples imply that two cases give an exact answer: a) when a sample is centered on the centroid, and b) when the centroid is exactly half-way between two samples. As the situation slides from case a) to case b), ... a shift equal to $T_s/2$, ... the systematic error increases from zero to its maximum value, and then returns to zero.

An Excel spreadsheet was used to calculate the systematic error in the computed centroid for the Gaussian peak. The test was implemented for a wide range of sampling intervals. In each case the position of the samples relative to the peak centroid was shifted in 8 steps of $T_s/8$, and the maximum difference between equation (4) and the true centroid was recorded as the maximum systematic error. The results are shown in Figure 4.

The horizontal axis in Figure 4 can be interpreted as the number of samples spanning the FWHM of the peak. The vertical axis defines the worst-case systematic error as a percent of the FWHM of the peak. Clearly, 1.27 samples across the FWHM is sufficient to render the systematic error less than 1% of the FWHM. Furthermore, the percent error plummets rapidly beyond the 1% point as the number of samples spanning the FWHM increases. In more practical terms, this means a sampling interval T_s = 2 ns will provide a systematic error <1% for peak widths >2.6 ns.

The systematic error will typically be less than the maximum error in Figure 4. For a particular peak in the spectrum, the systematic error will always be the same, no matter how many ions are collected in the peak or how many times the measurement is repeated. It is a systematic bias in the estimated centroid, t_c, arising from the asymmetry of the sample locations relative to the true centroid of the peak, T.

The same test was applied to the computation of the area from the sampled data points on the Gaussian peak.

$$A = T_s \sum_i V_i \qquad (5)$$

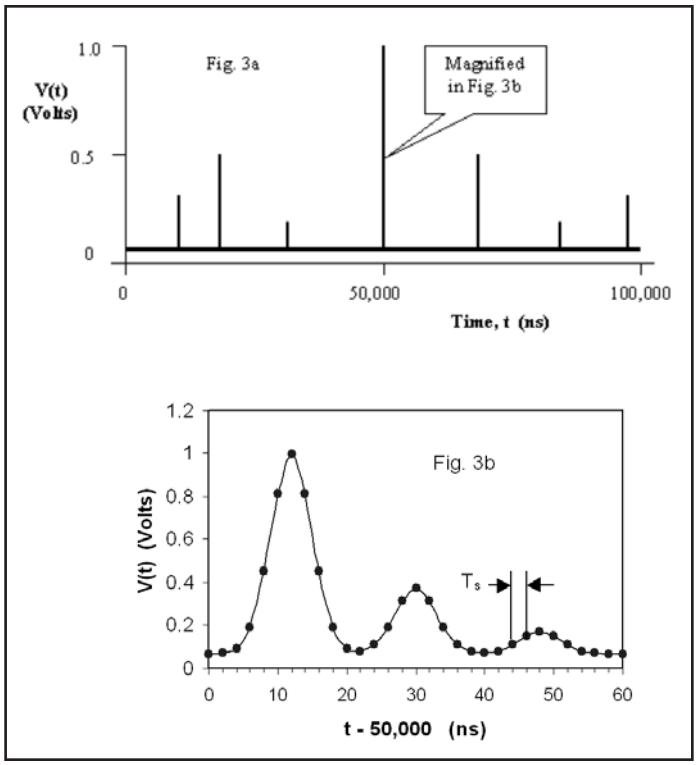

Figure 3. The record in the Summing Memory after completing one scan: a) the entire record, and b) a magnified view of the peaks at t ≈ 50,000 ns. The dots mark the ADC samples. In this case, the interval between samples is T_s = 2 ns. Continuous lines connect the dots to facilitate viewing.

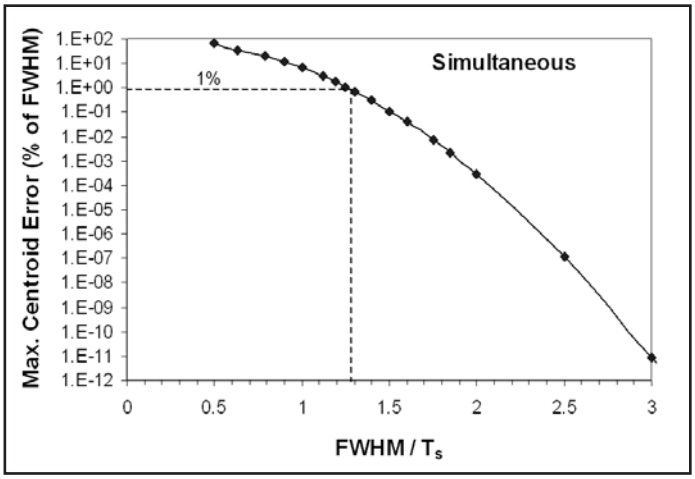

Figure 4. The maximum systematic centroid error due to an asymmetric alignment of the sampling interval relative to the true centroid of the Gaussian peak.

Figure 5 shows the maximum systematic bias in the value obtained for A from equation (5) as defined in equation (6).

$$Max.\ \%\ Error = \pm \frac{A_{max} - A_{min}}{A_{max} + A_{min}} \times 100\% \qquad (6)$$

where A_{max} and A_{min} are the maximum and minimum values obtained for the area of the peak from the sampling points. Note that the error is less than 1% if the number of data points across the FWHM is greater than 1.23. The systematic bias in the area of a specific peak will typically be less than the maximum specified in Figure 5. Moreover, that bias will always be the same for the area of that peak, no matter how many ions are collected in the peak or how many times the measurement is repeated.

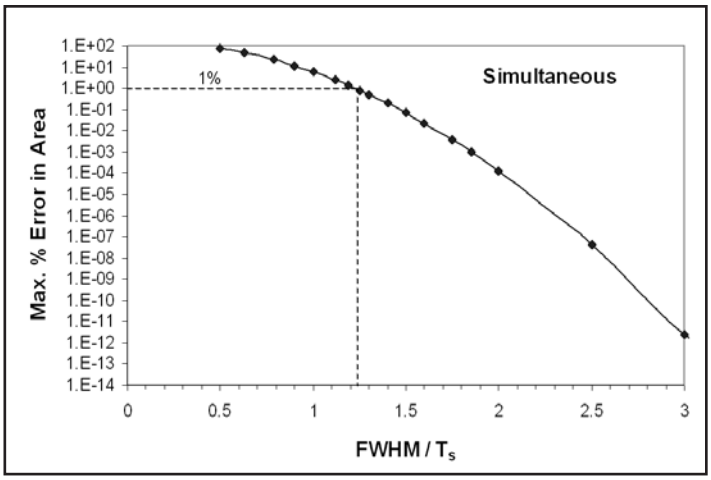

Figure 5. The systematic error in the estimated area caused by misalignment of the sampling interval relative to the centroid of the Gaussian peak.

Confirmation from the Nyquist Theorem

Oppenheim and Schafer have shown[2] that the original continuous analog signal can be reconstructed exactly from discrete digital samples by employing a universal interpolation function, provided the sampling frequency, $1/T_s$, exceeds twice the maximum frequency contained in the analog signal. This requirement on the sampling frequency is simply the Nyquist limit for avoiding aliasing of higher frequencies to a lower frequency.

The shape of the peaks in the analog signal can be represented in the time domain by the function

$$V(t) = \frac{(at)^n e^{-at}}{n!\, a^n} \qquad (7)$$

where the parameter, a, scales the width on the time axis, while n adjusts the shape. This function approaches a Gaussian shape for very large values of n. The example for n = 40 is illustrated in Figure 6. Note that the width at half maximum amplitude in units of "at" is 14.9. This means that the FWHM in units of time is

$$FWHM = \frac{W_{1/2}}{a} = \frac{14.9}{a} \qquad (8)$$

The function in equation (7) is convenient, because it has a simple Laplace Transform to describe the signal in the frequency domain[3]. In the complex frequency domain, the voltage as a function of frequency is described by v(iω) in equation (9).

$$v(i\omega) = \frac{1}{a^{n+1}\left(1 + \frac{i\omega}{a}\right)^{n+1}} \qquad (9)$$

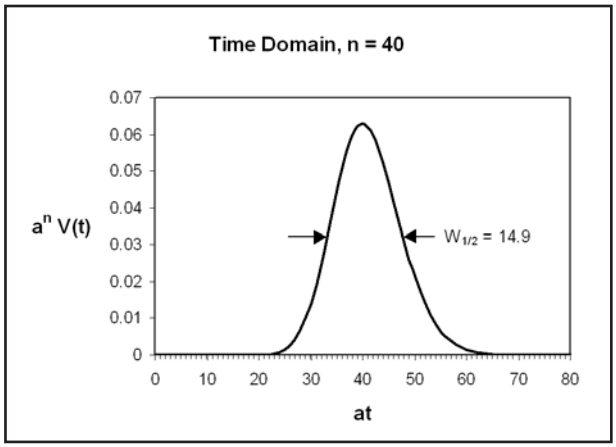

Figure 6. The analog pulse shape in the time domain, from equation (7).

where i is the square root of –1. The frequency, ω, in radians per second, is related to the frequency, f, in cycles per second by

$$\omega = 2\,\pi\, f \qquad (10)$$

The power density as a function of frequency is defined by multiplying v(iω) by its complex conjugate, v*(iω) to get

$$v(i\omega)\ \ v^*(i\omega) = \frac{1}{a^{2n+2}\left(1 + \frac{\omega^2}{a^2}\right)^{n+1}} \qquad (11)$$

The graph of equation (11) in Figure 7 plots the square of the amplitude of each frequency component comprising the peak.

The square root of the area under the curve in Figure 7 maps into the area under the peak in Figure 6 via the inverse Laplace Transform. If 0.99 of the area in Figure 6 is desired, that corresponds to $0.99^2 = 0.98$ of the area in Figure 7. Thus the frequency limit that incorporates 98% of the area in Figure 7 is determined from

$$\frac{\omega_{98\%}}{a} = 0.25 \qquad (12)$$

To satisfy the Nyquist limit, the sampling frequency must be greater than twice the limit in equation (12).

$$f_s \geq \frac{2\omega_{98\%}}{2\pi} = \frac{0.25\ a}{\pi} \qquad (13)$$

This guarantees that the errors from aliasing will be avoided on all but the 1% of the area in Figure 6 that corresponds to the highest frequencies. Substituting for "a" from equation (8), and noting that

$$f_s = \frac{1}{T_s} \qquad (14)$$

leads to the requirement

$$T_s \leq 0.843\ FWHM \qquad (15)$$

or

$$\frac{FWHM}{T_s} \geq 1.2 \qquad (16)$$

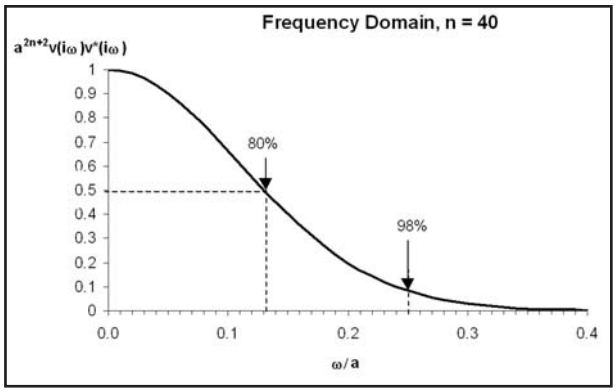

Figure 7. The power density distribution versus frequency for the peak in Figure 6. Only 2% of the power is contained in frequencies exceeding ω/a = 0.25.

The result in equation (16) is virtually identical to the limits derived by a completely different method in Figures 4 and 5. In order to limit the systematic error in peak position and area to <1%, the sampling interval must be small enough to have at least 1.2 to 1.27 samples covering a time interval equal to the FWHM of the peak.

The Random Error from Ion Counting Statistics

Independent of the sampling process examined above, there is a random uncertainty in the analog signal before it is sampled by the ADC. This uncertainty is a result of the random generation of ions at the source. If the number of ions, N, in a peak is repeatedly measured, the number N will vary randomly about a central value from measurement to measurement.

If the ionized molecules detected in a specific peak are summed over a finite time period, t, the Poisson Distribution, P(N), describes the probability of detecting N ions[4, 5, 6] in that single measurement of duration, t.

$$P(N) = \frac{\mu^N e^{-\mu}}{N!} \qquad (17)$$

If the measurement is repeated a large number of times and the values of N are averaged, the average value of N approaches the mean of the distribution, μ, as the number of repeated measurements approaches infinity. Note that the Poisson Distribution has a standard deviation

$$\sigma_N = \sqrt{\mu} \approx \sqrt{N} \qquad (18)$$

Substituting N for μ in equation (18) recognizes that the value of N from a single measurement is an adequately accurate estimate[5] of μ.

A more useful description of the precision of the measurement is obtained by multiplying the relative standard deviation, σN / N, by 100% to express the percent standard deviation as

$$\sigma_N\ \% = \frac{\sigma_N}{N}\ x\ 100\% = \frac{100\%}{\sqrt{N}} \qquad (19)$$

Table 1 shows how the percent standard deviation improves as the counted number of events increases.

Clearly, a large number of events must be accumulated to achieve a random error lower than 1%.

Table 1. σ_N% for Selected Values of N.

N	σ_N%
1	100.0%
100	10.0%
10,000	1.0%
1,000,000	0.1%

The Random Error from Detector Gain Statistics

Because a digital signal averager responds linearly to the amplitude of the analog signal, it is sensitive to the variance in the gain of the microchannel plate detector. This variance is inherent in the analog signal before it is sampled by the ADC. Thus, it is independent of the sampling process. The area A within a peak in the time-of-flight spectrum is controlled by

$$A = N\,G_d\,G_p \qquad (20)$$

where N is the number of ions detected, G_d is the gain of the microchannel plate detector, and G_p is the gain of the preamplifier. The variance in A can be calculated as[5, 6]

$$\sigma_A^2 = \left(\frac{\partial A}{\partial N}\right)^2 \sigma_N^2 + \left(\frac{\partial A}{\partial G_d}\right)^2 \sigma_{Gd}^2 + \left(\frac{\partial A}{\partial G_p}\right)^2 \sigma_{Gp}^2 \qquad (21)$$

$$= (G_d\,G_p)^2\,\sigma_N^2 + (N\,G_p)^2\,\sigma_{Gd}^2 + (N\,G_d)^2\,\sigma_{Gp}^2$$

Dividing equation (21) by the square of equation (20) yields

$$\left(\frac{\sigma_A}{A}\right)^2 = \left(\frac{\sigma_N}{N}\right)^2 + \left(\frac{\sigma_{Gd}}{G_d}\right)^2 + \left(\frac{\sigma_{Gp}}{G_p}\right)^2 \qquad (22)$$

Because the preamplifier has a stable gain and a high signal-to-noise ratio, the third term on the right in equation (22) is negligible compared to the other two. Consequently, it can be ignored. Using that fact and substituting from equation (18) simplifies equation (22) to

$$\left(\frac{\sigma_A}{A}\right)^2 = \left(\frac{1}{N}\right) + \left(\frac{\sigma_{Gd}}{G_d}\right)^2 \qquad (23)$$

For a practical result, an evaluation of the last term in equation (23) is required. This can be accomplished by noting that the output pulse from the microchannel plate detector has an area equal to the charge in the pulse, q. If q is measured in terms of the number of electrons in the output pulse, then the gain of the detector is

$$G_d = q \qquad (24)$$

In other words, each electron injected into the cathode of the detector produces q electrons at the output from the anode of the microchannel plate detector. To obtain a linear response, the microchannel plate is typically operated in its linear (unsaturated) mode when used with a digital signal averager. For a single electron injected at the cathode, the output charge, q, has a probability distribution given by[7, 8]

$$P_1(q) = k\,e^{-kq} \qquad (25)$$

when operated in the linear mode. This distribution has a mean[5]

$$q_{mean} = \int_{q=0}^{\infty} q\,P_1(q)\,dq = \frac{1}{k} \qquad (26)$$

which defines the constant k. The variance of the distribution is[5]

$$\sigma_q^2 = \int_{q=0}^{\infty} q^2\,P_1(q)\,dq = \frac{1}{k^2} = (q_{mean})^2 \qquad (27)$$

But, what is needed is the probability distribution for N_e electrons injected into the cathode. This can be derived by performing a convolution of the distribution from equation (25) with itself, where the convolution is of order N_e. This convolution is most easily computed[5] by taking the Laplace transform of equation (25), which is[3]

$$L\{P_1(q)\} = \frac{k}{s+k} \qquad (28)$$

where s is the complex variable corresponding to 1/q. Now, the convolution of order N_e is simply

$$(L\{P_1(q)\})^{Ne} = \left(\frac{k}{s+k}\right)^{Ne} = L\{P_{Ne}(q)\} \qquad (29)$$

The inverse Laplace transform of the expression in equation (29) produces[3]

$$P_{Ne}(q) = \frac{k^{Ne}\, q^{Ne-1}\, e^{-kq}}{(N_e - 1)!} \qquad (30)$$

$P_{Ne}(q)$ is the probability distribution for the total charge q in the output pulse from the microchannel plate detector when N_e electrons have been collected by the cathode of the detector for a specific peak in the time-of-flight spectrum. The distribution has a mean

$$Q_{mean} = \int_{q=0}^{\infty} q\ P_{Ne}(q)\, dq = \frac{N_e}{k} = N_e\, q_{mean} \qquad (31)$$

and a variance

$$\sigma_Q^2 = \int_{q=0}^{\infty} q^2\, P_{Ne}(q)\, dq = \frac{N_e}{k^2} = N_e\, \sigma_q^2 = N_e\, q_{mean}^2 \qquad (32)$$

Equation (30) is illustrated in Figure 8 for $N_e = 1$ and $N_e = 9$.

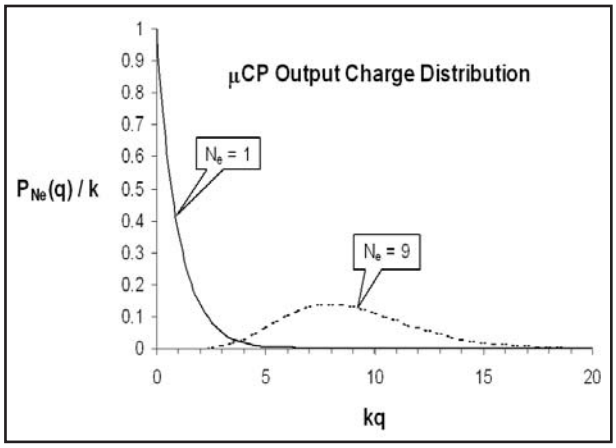

Figure 8. The output charge distribution from a microchannel plate detector operated in the linear mode for $N_e = 1$ electron and $N_e = 9$ electrons injected at the cathode.

Equations (31) and (32) permit the last term in equation (23) to be written as

$$\left(\frac{\sigma_{Gd}}{G_d}\right)^2 = \frac{\sigma_Q^2}{Q_{mean}^2} = \frac{N_e\, q_{mean}^2}{(N_e\, q_{mean})^2} = \frac{1}{N_e} \qquad (33)$$

For more meaning, it is useful to express N_e in terms of the number of ions, N, collected by the detector cathode and the average number of electrons injected into the detector by each ion, n_e.

$$N_e = N\, n_e \qquad (34)$$

Substituting equations (33) and (34) into equation (23), taking the square root, and multiplying by 100% leads to the expression for the combined random error from ion counting and gain statistics in equation (35).

$$\sigma_A\% = \frac{\sigma_A}{A} \times 100\% \qquad (35)$$

$$= \frac{\sqrt{1 + \left(\frac{1}{n_e}\right)\left(\frac{\sigma_q}{q_{mean}}\right)^2}}{\sqrt{N}} \times 100\%$$

$$= \frac{\sqrt{1 + \left(\frac{1}{n_e}\right)}}{\sqrt{N}} \times 100\%$$

Note that when the number of electrons per ion, n_e, becomes large compared to 1, the contribution from gain statistics becomes negligible, and only the uncertainty from ion counting statistics remains (see equation (19)). This is the best case. The worst case is when $n_e = 1$, and equation (35) produces a percent standard deviation that is 1.41 times the uncertainty from ion counting statistics alone.

Equation (35) is plotted in Figure 9 for $n_e = 1$ and $n_e = 100$. Note that equation (35) and Figure 9 can be applied to the area of a single pulse from the detector, or to the area of a peak in the time-of-flight spectrum that has been acquired over a period of time.

The Importance of the Impulse Response

The impulse response is the pulse produced in response to one ion arriving at the cathode of the detector. It is important because it can contribute to the width of the peak in the time-of-flight spectrum if its width is not small compared to the jitter in ion arrival times. It is also a useful concept for computing the random error in the peak centroid.

Figure 10 illustrates the impulse responses at different points in the system. Although these pulses actually have a negative polarity, they have been inverted and drawn as positive pulses in Figure 10 for ease of viewing. Additionally, the amplitudes have been artificially adjusted to the same value to facilitate comparisons of the pulse widths.

A single ion arriving at the cathode of the microchannel plate detector produces the typical pulse shape designated "µCP" in Figure 10. It has a rise time of 250 ps and a 350-ps FWHM. At the output of the preamplifier, this pulse has broadened to a 700-ps FWHM. The bandwidth limit in the input to the ADC in the digital signal averager broadens the FWHM further to about 1.0 ns. This final analog impulse response at the "ADC Input" includes the minor smearing effect of the sampling aperture, ΔT_s, of the ADC. If this smearing is assigned to the analog impulse response it permits the sampling aperture to be treated as though it is infinitesimal, ... as has been done throughout this application note.

Due to imperfections in the ion optics of the time-of-flight mass spectrometer, all ions with the same value of m/z do not experience exactly the same flight time. The distribution of flight times is quasi-Gaussian, with a jitter defined by the standard deviation σ_{ft} for the distribution. This flight-time distribution is convolved with the impulse response at the ADC input to produce the shape of the peak sampled in the digital signal averager. For a peak that contains multiple ions, the width of the peak recorded in the spectrum can be characterized by the standard deviation, σ_M, as defined in equation (36).

$$\sigma_M = \sqrt{\sigma_{ft}^2 + \sigma_I^2} \qquad (36)$$

where σ_I is the standard deviation of the impulse response at the ADC input. If both the flight time distribution and the impulse response are approximately Gaussian in shape, the relationship between the FWHM, W, and the standard deviation, σ, is

$$W = 2.35\,\sigma \qquad (37)$$

Although not absolutely essential, this allows equation (36) to be cast in the convenient form

$$W_M = \sqrt{W_{ft}^2 + W_I^2} \qquad (38)$$

where W_M, W_{ft}, and W_I are the FWHM values corresponding to σ_M, σ_{ft}, and σ_I respectively. The existence of the impulse response broadens the peak in the spectrum. But this broadening will be less than 12% if $\sigma_{ft} > 2\,\sigma_I$. Table 2 demonstrates this principle for practical values. W_{ft} is the FWHM jitter in the ion flight times, W_M is the FWHM of the peak actually recorded in the spectrum, and W_I is the FWHM of the impulse response.

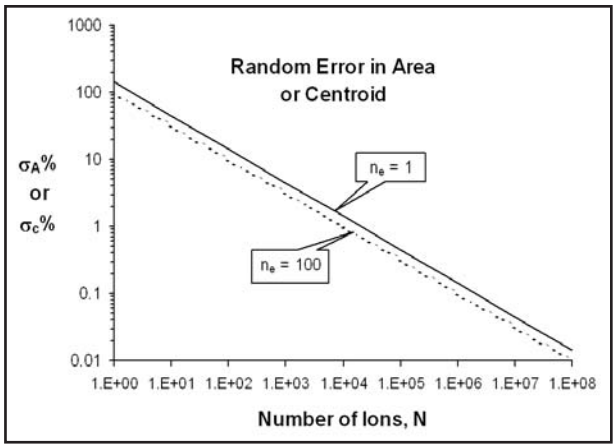

Figure 9. The percent random error in the area of a peak, σ_A%, resulting from ion counting statistics and detector gain statistics. The two curves represent the worst and best cases, i.e., $n_e = 1$ electron and $n_e = 100$ electrons injected into the detector by an ion. The graph also applies to σ_c%, the random error in the peak centroid expressed as a percent of the standard deviation in the ion flight times.

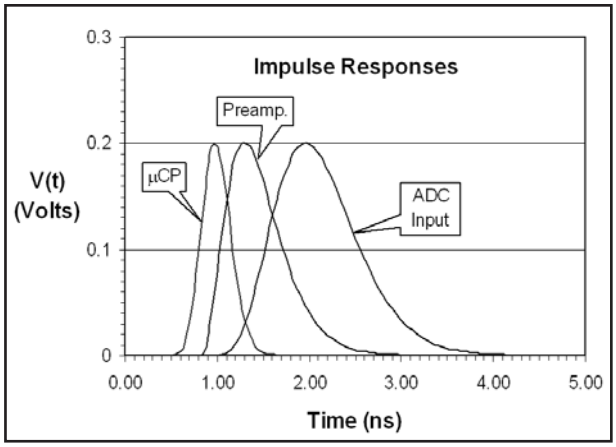

Figure 10. Impulse responses at three points in the analog signal processing chain: the output of the microchannel plate detector (µCP), the preamplifier output, and the input to the sampling ADC in the digital signal averager. The pulse shapes are the response to a single ion striking the detector. The polarities have been inverted and the amplitudes adjusted to simplify the depiction.

Table 2. Peak Broadening for W_I = 1 ns

W_{ft} (ns)	W_m (ns)	W_m / W_{ft}
1	1.41	1.41
2	2.24	1.12
3	3.16	1.05
4	4.12	1.03
5	5.10	1.02
6	6.08	1.01

The Random Error in the Centroid of the Peak

Random fluctuations in a) the ion flight times, b) the number of ions and c) the detector gain also cause random fluctuations in the mean arrival time of the analog pulse before it is sampled by the ADC. The resulting random error in the centroid of the peak is independent of the sampling process. To develop the equations, consider the hypothetical situation where the impulse response of each ion can be recorded in a separate memory as that ion arrives. After N ions have been collected in a particular peak in the time-of-flight spectrum, the impulse response of each contributing ion can be examined to determine its area, α_i, and centroid, t_{ci}. The centroid of the peak resulting from combining the impulse responses from the N ions is computed from

$$t_C = \frac{1}{A} \sum_{i=1}^{N} \alpha_i \, t_{ci} \qquad (39)$$

where the area of the resultant peak is

$$A = \sum_{i=1}^{N} \alpha_i \qquad (40)$$

The time distribution of the impulse response centroids, t_{ci}, is a sampling of the ion flight-time distribution. This flight-time distribution has a variance defined by

$$\sigma_{ft}^2 = \frac{1}{A} \sum_{i=1}^{N} \alpha_i \, (t_{ci} - t_C)^2 \qquad (41)$$

The statistical uncertainty in the computed value of the centroid, t_c, is caused by the statistical variance in the αi in equations (39) and (40). The area, αi, is related to the number of ions causing the pulse by analogy with equation (20), i.e.,

$$A = N \, G_d \, G_p \qquad (20)$$

$$\alpha i = n_i \, G_d \, G_p \qquad (42)$$

where n_i is the number of ions causing area α_i. By definition, $n_i = 1$, because α_i is the area of the impulse response. But, n_i will be carried through the development of the equations until it automatically disappears.

By analogy with equation (35), the standard deviation in α_i is

$$\sigma_{\alpha i} = \frac{\beta}{\sqrt{n_i}} \, \alpha_i \qquad (43)$$

where

$$\beta = \sqrt{1 + \left(\frac{1}{n_e}\right)} \qquad (44)$$

Using equation (42), equation (43) can be modified to

$$\sigma_{\alpha i}^2 = \frac{\beta^2 \, \alpha_i^2}{\left(\frac{\alpha_i}{G_d \, G_p}\right)} = G_d \, G_p \, \beta^2 \, \alpha_i \qquad (45)$$

Moving back to equation (39), the variance in t_c is calculated from[5, 6]

$$\sigma_{tC}^2 = \sum \left(\frac{\partial t_C}{\partial \alpha_i}\right)^2 \sigma_{\alpha i}^2 \qquad (46)$$

The partial derivative can be simplified to

$$\frac{\partial t_C}{\partial \alpha_i} = \frac{t_{ci} \left(\sum_{i=1}^{N} \alpha i\right) - \sum_{i=1}^{N} \alpha_i t_{ci}}{A^2} \equiv \frac{t_{ci} - t_C}{A} \qquad (47)$$

Consequently, substituting equations (45) and (47) in (46) yields

$$\sigma_{tC}^2 = \frac{G_d\, G_p\, \beta^2}{A} \sum_{i=1}^{N} \frac{\alpha_i\, (t_{ci} - t_C)^2}{A} = \frac{G_d\, G_p\, \beta^2}{A}\, \sigma_{ft}^2 \qquad (48)$$

Substituting for A from equation (20) in equation (48), taking the square root, rearranging , and multiplying by 100%, leads to the simple answer

$$\sigma_C\% = \frac{\sigma_{tC}}{\sigma_{ft}} x\ 100\% = \frac{\sqrt{1 + \left(\frac{1}{n_e}\right)}}{\sqrt{N}}\ x\ 100\% \qquad (49)$$

Equation (49) expresses the random error in the peak position as a percent of the jitter in the ion flight time. Note that the right side of equation (49) is identical to the right side of equation (35). For that reason, Figure 9 applies to both percent random errors: σ_A% for the peak area, and σ_C% for the peak centroid. Note also that it requires more than 20,000 ions counted in the peak to reduce either random error below 1% if $n_e = 1$.

What is the Meaning of "Random" and "Systematic"?

Systematic Errors are biases in the answer that remain the same, no matter how many times the measurement is repeated. Systematic errors can be eliminated by calibration with a reference standard. An example is the adjustment of the elevation angle of a cannon to hit a target that it has been systematically missing at a 2-km distance.

Random Errors occur when the answers vary unpredictably from measurement to measurement around some central value. An example is the scatter in the points of impact of the cannon balls around the target at a 2-km distance. Random errors can be reduced by repeating the measurement n times, and calculating the average. Although that tactic is not very useful in the cannon example, it is beneficial in many scientific measurements. If σ_1 is the random error (standard deviation) in a single measurement, then the standard deviation in the average of n measurements is[5, 6]

$$\sigma_n = \frac{\sigma_1}{\sqrt{N}} \qquad (50)$$

The error resulting from asymmetric alignment of the sampling interval with respect to the centroid of the peak is a *systematic* error, i.e., a bias in the answer. This systematic bias is independent of the random error. In other words, it remains constant for a specific peak, no matter how many ions are collected in the peak or how many times the measurement is repeated. However, if the systematic error is small compared to the random error, its magnitude will be obscured by the random error. If the measurement is averaged a sufficient number of times to make the random error negligible compared to the systematic error, the now-evident systematic error can be canceled by an appropriate calibration curve or look-up table.

The fluctuations in a) the ion flight times, b) the number of ions detected, and c) the detector gain all contribute to the *random* error. As equations (35) and (49) reveal, the random error can be reduced by increasing the number of electrons released at the detector cathode, increasing the number of ions in each pulse, or averaging more scans. The function of a signal averager is to reduce the random error or noise by averaging a large number of repetitive measurements, so that the systematic shape of the signal can be extracted from the noise. For the system illustrated in Figure 1, this averaging takes place in both the analog and digital electronics. Analog averaging is achieved in the detector by summing the responses from N ions and n_e electrons in a single pulse. Digital averaging is achieved in the digital signal averager by summing a large number of records in the memory to form each reported spectrum.

Which Error Dominates?

It is informative to separate the operation of the TOF-MS into two domains: one where the random error from ion and gain statistics dominates, and the other where the systematic sampling error dominates. This can be achieved by choosing a value for the sampling interval, T_s, noting the systematic sampling error, and finding the number of ions, N, that produces a random error equal to the sampling error. Successive pairs of values are plotted as N versus T_s. The line on the resulting graph represents the approximate boundary between the domain where the random error from ion and gain statistics dominates, and the domain where the systematic sampling error dominates. Figure 11 shows the results for combining the data from Figures 4 and 9 for the centroid, while Figure 12 illustrates the results of combining Figures 5 and 9 for the area.

Note that the parameter on the horizontal axis has been inverted from "FWHM / T_s" to "T_s / FWHM" in order to define the dominance domains. Also, the data for σ_C% from Figure 9 has been divided by 2.35 for an approximate conversion to a percent of the FWHM, ...

with the further presumption that the impulse response broadens the peak by a negligible amount. These approximations are adequate for the definition of the fuzzy boundary between the two domains.

The normal operating range of a digital signal averager in a TOF-MS is mapped in the gray rectangle found in the lower left corner of both graphs. The maximum limit on the horizontal axis comes from the 1% limit defined in Figures 4 through 7, i.e., T_s / FWHM ≈ 1/1.3 = 0.77. The left limit is based on T_s = 0.5 ns and FWHM = 10 ns. The lower and upper limits of the rectangle on the vertical axis are 1 and 10^7 ions, respectively. The latter is a rather aggressive limit for the number of ions accumulated in a single peak when the TOF-MS is fed by a chromatograph. It requires 1,000 ions in the peak per acceleration pulse at a 10-kHz repetition rate for 1 second.

It is obvious from Figures 11 and 12 that the random error from ion and gain statistics is the dominant error over the vast majority of the operating range of a TOF-MS. The exception is the small upper right corner of the gray rectangle. In the Centroid graph, the curved boundary for this corner corresponds to the random and systematic errors simultaneously transitioning from 0.7% of the FWHM to 0.02% of the FWHM. If the spectrometer is discovered to be operating in this corner, simply decreasing the sampling interval by a factor of two will render the systematic sampling error negligible compared to the random error from ion and gain statistics.

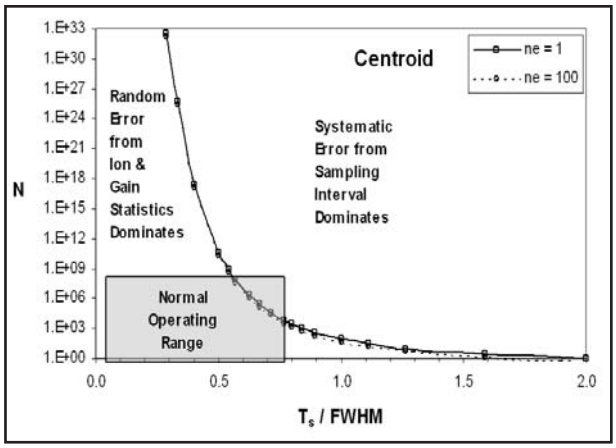

Figure 11. The normal operating range of the digital signal averager with a TOF-MS, and the two dominant error domains for measurement of the peak centroid.

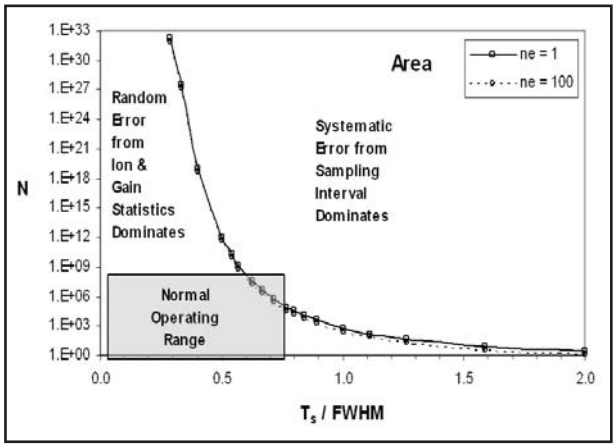

Figure 12. The normal operating range of the digital signal averager with a TOF-MS, and the two dominant error domains for measurement of the peak area.

Interleaving for Higher Sampling Rates

At the time this application note was written, the maximum sampling rate for readily-available, 8-bit, flash ADCs was 500 MS/s. This corresponds to a minimum sampling interval, T_s = 2 ns. Peak widths in a TOF-MS typically range from 3 to 10 ns. Although, 2-ns sampling has already been shown to extract all the valuable information on peak position and area, it is easier to visualize the shape of the narrowest peaks if the sampling frequency is increased to 2 GS/s. There are two ways to achieve 2-GS/s sampling with a 500-MS/s ADC. Method I uses a single ADC with programmed offsets of the trigger delay[9]. Method II employs four ADCs operating in parallel from a common sampling clock, with the clock shifted by 0.5-ns increments for sampling each of the four ADCs. The two methods are compared and contrasted below.

Method I: Single ADC with Programmed Trigger Offsets

This method uses the scheme depicted in Figure 2 to achieve the interleaving illustrated in Figure 13. It uses four scans to acquire one interleaved record. Each scan is synchronized with its own acceleration pulse[9]. The averager memory is divided into four separate memories. Each scan samples at 2-ns intervals. During the first scan, the samples denoted by the solid squares in Figure 13 (Series 1) are acquired in Memory 1. For the second scan, the Trigger Delay is reduced by 0.5 ns, and the samples represented by the + signs (Series 2) are stored in Memory 2. On the third scan, the Trigger Delay is decreased by another 0.5 ns, and the samples depicted by the circles (Series 3) are collected in Memory 3. For the fourth scan, the Trigger Delay is lowered by another 0.5 ns, and the samples marked with an x (Series 4) are saved in Memory 4. On the fifth scan the Trigger Delay is increased by 1.5 ns (back to its original value), and the cycle of four scans is repeated with the new samples being added to the previous samples in the respective memories. This process continues until the desired number of records has been summed. At the end of the acquisition, the four memories are read, and the data are interleaved to form the spectrum illustrated in Figure 13.

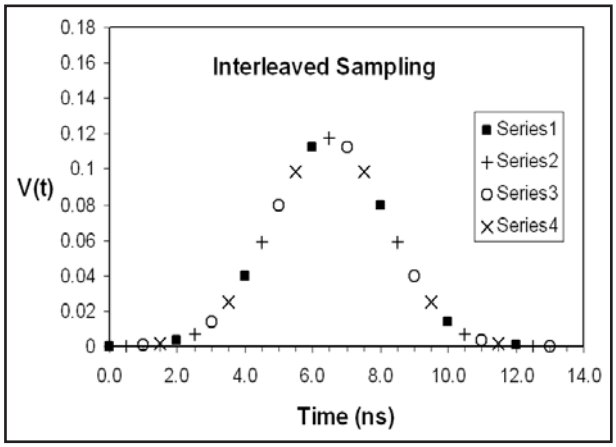

Figure 13. An illustration of interleaved sampling with a 500-MS/s ADC to achieve 2-GS/s sampling.

Method II: Four ADCs with Clock Offsets

This scheme essentially uses four digital signal averagers, all operating in parallel from the same sampling clock, and all using the same trigger. Each ADC takes samples at 2-ns intervals. The analog signal is applied simultaneously to all four inputs. The sampling clock is fed to ADC 1with zero delay, and that digital signal averager collects the samples marked by the solid squares in Figure 13 (Series 1). The sampling clock is delayed by 0.5 ns before it is applied to ADC 2, and that ADC acquires the samples depicted with + signs (Series 2). Next, the clock is delayed by an additional 0.5 ns before being applied to ADC 3, and that ADC records the samples labeled with a circle (Series 3). Finally, the sampling clock is delayed by yet another 0.5 ns before strobing ADC 4 to accumulate the samples marked with an x (Series 4). Each input sums the desired number of records. At the end of the process, the four memories are read, and the data are interleaved to yield the complete spectrum as illustrated in Figure 13.

Because Method II requires a four-fold duplication of the basic digital signal averager, the cost of Method II is 3 to 4 times the cost of Method I. Method II has another drawback. It is essentially impossible to exactly match the dc offsets, gains, and bit boundaries of the four ADCs. The result is a choppy pattern superimposed on the amplitudes. In principle, one can write a program to map the codes from ADCs 2, 3, and 4 to match the code from ADC 1. But, this mapping must be performed on the entire record at the end of each scan. As a result, Method II spends more than 90% of the available time mapping the code corrections. This leaves less than 10% of the time for data acquisition.

Method II does have the advantage of being able to acquire a single interleaved record in one scan, whereas Method I requires four scans. However, the percent random error from ion and gain statistics is so large that a single scan is never enough in time-of-flight mass spectrometry. A large number of scans must be summed to achieve an acceptable random error.

How do Methods I and II compare with respect to precision? That question is answered in the next two sections.

Random Error: Method I vs. Method II

As Figures 11 and 12 demonstrate, the dominant error is virtually always the random error from ion and gain statistics. Therefore, that source of error is the most important to compare between the two methods. The random error is inherent in the analog signal before sampling by the ADC, and is independent of the sampling process.

Method I: Consider a single scan during which N_1 ions are collected in a specific peak. Equations (35), (44), and (49) define the percent random errors in the centroid and area of the peak as

$$\sigma_C\%|_{I1} = \frac{\beta}{\sqrt{N_1}} x\ 100\% \qquad (51)$$

$$\sigma_A\%|_{I1} = \frac{\beta}{\sqrt{N_1}} x\ 100\% \qquad (52)$$

Where the vertical line with an "I1" subscript means that result is specific to Method I with one scan completed. But, it takes 4 scans to form a complete, interleaved record with 0.5-ns sampling intervals. Each of the 4 scans contains N_1 ions in the peak. When the 4 scans are combined to form the interleaved record, the total number of ions incorporated in the peak is 4 N_1, and the random errors become

$$\sigma_C\%|_{I4} = \frac{\beta}{\sqrt{4N_1}}\ x\ 100\% \qquad (53)$$

$$\sigma_A\%|_{I4} = \frac{\beta}{\sqrt{4N_1}}\ x\ 100\% \qquad (54)$$

The subscripts on the vertical lines in equations (53) and (54) imply "Method I with 4 scans".

Method II: It takes only one scan with the four ADCs to form one complete record. At the end of this scan the peak will contain N_1 ions, and the random errors are

$$\sigma_C\%|_{II4} = \frac{\beta}{\sqrt{N_1}}\ x\ 100\% \qquad (55)$$

$$\sigma_A\%|_{II4} = \frac{\beta}{\sqrt{N_1}}\ x\ 100\% \qquad (56)$$

where the subscripts on the vertical lines designate "Method II with 1 scan". Clearly, it is going to require 4 scans with Method II to equal the random errors inherent in one complete record from Method I. The random errors for 4 scans with Method II are

$$\sigma_C\%|_{II4} = \frac{\beta}{\sqrt{4N_1}} \; x\; 100\% \qquad (57)$$

$$\sigma_A\%|_{II4} = \frac{\beta}{\sqrt{4N_1}} \; x\; 100\% \qquad (58)$$

Equations (57) and (58) exactly match equations (53) and (54).

CONCLUSION: *The same number of scans is required with Method I and Method II to achieve the same random errors in the centroid and the area of the peak. Neither method has an advantage with respect to the number of scans.*

Systematic Sampling Error: Method I vs. Method II

To examine the systematic bias arising from an asymmetric alignment of the sampling interval with respect to the true centroid of the peak, T, the random error must be made negligible so that it does not obscure the systematic peak shape. The task is to find the sampled centroid, t_C, and determine its systematic deviation from the true centroid, T (see equations (2), (3) and (4)). Consider a well-defined peak that will ultimately be reconstructed from 4n sequentially ordered samples that produce a set of sampled voltages, V_i, corresponding to the sampling times, t_i. The segment of area from the peak estimated by each sample is given by

$$a_i = T_s\, V_i \qquad (59)$$

The total area of the peak is calculated from

$$A = a_1 + a_2 + a_3 + a_4 + a_5 + \ldots\ldots\ldots\ldots + a_{4n-3} + a_{4n-2} + a_{4n-1} + a_{4n} = \sum_{i=1}^{4n} a_i \qquad (60)$$

and the sampled centroid is computed from

$$t_C = \frac{1}{A}\sum_{i=1}^{4n} a_i\, t_i \qquad (61)$$

As developed earlier, Figure 4 shows the maximum systematic deviation of t_C from the true value of the peak's centroid, T, as a function of FWHM / T_s. Additionally, Figure 5 graphs the maximum systematic deviation of A as a function of FWHM / T_s. Now modify the process to fit Methods I and II .

Method I

Method I acquires the samples in four separate scans. Samples a_1, a_5, a_9, ... , a_{4n-3} are collected in Memory 1 during the first scan, samples a_2, a_6, a_{10}, ... , a_{4n-2} are stored in Memory 2 during the second scan, samples a_3, a_7, a_{11}, ... , a_{4n-1} are saved in Memory 3 during the third scan, and samples a_4, a_8, a_{12}, ... , a_{4n} are deposited in Memory 4 during the fourth scan.

After the four scans have been completed, the areas from each of the four memories can be extracted as A_1, A_2, A_3, and A_4, corresponding to memories 1, 2, 3, and 4. The results are

$$A_1 = a_1 + a_5 + a_9 + \ldots\ldots\ldots\ldots + a_{4n-3} = \sum_{j=1}^{n} a_{4j-3} \qquad (62a)$$

$$A_2 = a_2 + a_6 + a_{10} + \ldots\ldots\ldots\ldots + a_{4n-2} = \sum_{j=1}^{n} a_{4j-2} \qquad (62b)$$

$$A_3 = a_3 + a_7 + a_{11} + \ldots\ldots\ldots\ldots + a_{4n-1} = \sum_{j=1}^{n} a_{4j-1} \qquad (62c)$$

$$A_4 = a_4 + a_8 + a_{12} + \ldots\ldots\ldots\ldots + a_{4n} = \sum_{j=1}^{n} a_{4j} \qquad (62d)$$

Similarly, the centroid of the peak is extracted from each of the four memories according to

$$t_{C1} = \frac{1}{A_1}\sum_{j=1}^{n} a_{4j-3}\, t_{4j-3} \qquad (63a)$$

$$t_{C2} = \frac{1}{A_2}\sum_{j=1}^{n} a_{4j-2}\, t_{4j-2} \qquad (63b)$$

$$t_{C3} = \frac{1}{A_3} \sum_{j=1}^{n} a_{4j-1}\, t_{4j-1} \qquad (63c)$$

$$t_{C4} = \frac{1}{A_4} \sum_{j=1}^{n} a_{4j}\, t_{4j} \qquad (63d)$$

The areas and centroids from the four memories are combined via equations (64) and (65) to get the grand area, A, and the grand centroid, t_C.

$$A = A_1 + A_2 + A_3 + A_4 \qquad (64)$$

$$t_C = \frac{1}{A} (A_1\, t_{c1} + A_2\, t_{c2} + A_3\, t_{c3} + A_4\, t_{c4}) \qquad (65)$$

The task is to determine the extent to which t_C from equation (65a) systematically deviates from the true centroid, T, if the sampling interval is not symmetric about the true centroid. Similarly, the systematic deviation of A from equation (64a) is sought when symmetry is not fulfilled. The maximum systematic errors in the centroid and the area were determined using the same Excel spreadsheet process that was used for Figures 4 and 5, except the steps outlined in equations (62) through (65) were employed, instead of calculating A and t_C directly from one grand set of samples. The results are displayed in Figures 14 and 15. These two figures show the maximum systematic sampling errors for interleaving 4 scans, each having sampling intervals of $4T_s$, to form one record with a sampling interval, T_s.

Note that Figures 14 and 15 are identical to Figures 4 and 5. Interleaved sampling produces the same systematic sampling error as simultaneous sampling. Although this may seem surprising, it should not be. Aeronautical and Automotive Engineers commonly use the principle that the center of gravity of an assembly of parts can be calculated from the centers of gravity of its component parts.

A mathematical analysis produces a more rigorous explanation. The terms in equations (64a) and (65a) for calculating the grand area and the grand centroid from the areas and centroids of each individual group can be simply rearranged to show that they are identical to equations (60) and (61)

$$A = A_1 + A_2 + A_3 + A_4 \qquad (64a)$$

$$= \sum_{j=1}^{n} a_{4j-3} + \sum_{j=1}^{n} a_{4j-2} + \sum_{j=1}^{n} a_{4j-1} + \sum_{j=1}^{n} a_{4j}$$

$$= (a_1 + a_5 + \ldots + a_{4n-3}) + (a_2 + a_6 + \ldots + a_{4n-2}) + (a_3 + a_7 + \ldots + a_{4n-1}) + (a_4 + a_8 + \ldots + a_{4n})$$

$$= a_1 + a_2 + a_3 + a_4 + a_5 + a_6 + a_7 + a_8 + \ldots + a_{4n-3} + a_{4n-2} + a_{4n-1} + a_{4n}$$

$$= \sum_{i=1}^{4n} a_i \qquad (64b)$$

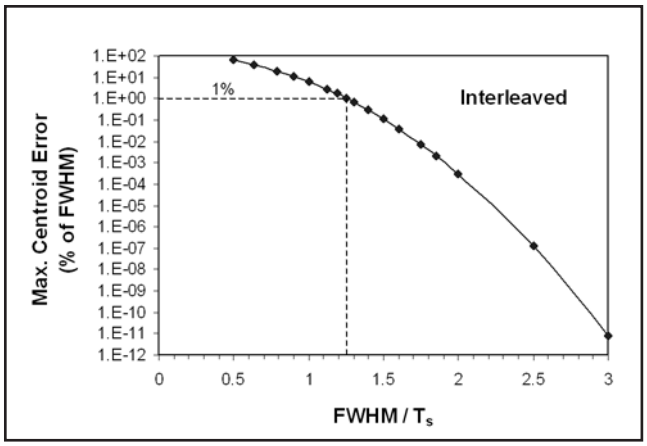

Figure 14. The maximum centroid error for the peak resulting from misalignment of the sampling intervals with respect to the centroid of the peak when interleaved sampling is employed.

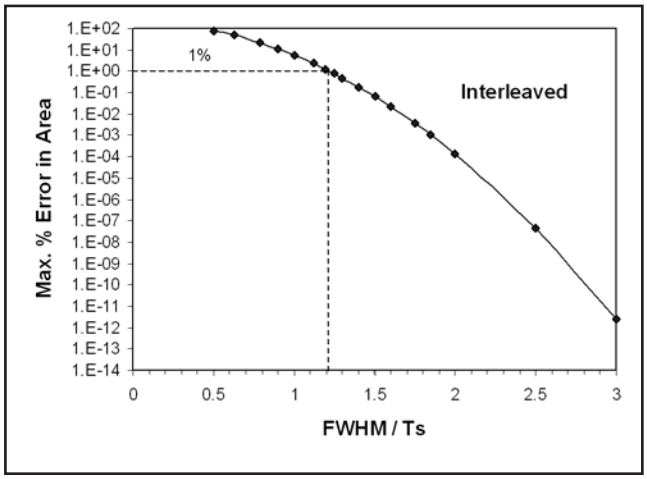

Figure 15. The maximum percent error in the area of the peak resulting from misalignment of the sampling intervals with respect to the centroid of the peak when interleaved sampling is employed.

$$t_C = \frac{1}{A}\ (A_1\ t_{c1} + A_2\ t_{c2} + A_3\ t_{c3} + A_4\ t_{c4}) \qquad (65a)$$

$$= \frac{1}{A}\left(\frac{A_1}{A_1}\sum a_{4j-3}\ t_{4j-3} + \frac{A_2}{A_2}\sum a_{4j-2}\ t_{4j-2} + \frac{A_3}{A_3}\sum a_{4j-1}\ t_{4j-1} + \frac{A_4}{A_4}\sum a_{4j}\ t_{4j}\right)$$

$$= \frac{1}{A}\sum_{i=1}^{4n} a_i\ t_i \qquad (65b)$$

Note that the last lines of equations (64b) and (65b) are identical to equations (60) and (61), respectively. Therefore, the sampled centroid calculated from equation (65) will produce exactly the same value as the sampled centroid calculated from equation (61). Consequently, the deviation from the true centroid, T, will be the exactly the same for both cases. It doesn't matter whether the samples are acquired as one continuous set of 4n samples, or as four separate sets of n samples on four separate scans. The results are identical either way. The same conclusions can be drawn concerning the systematic sampling error for the area.

CONCLUSION: *For calculation of the centroid and area of the peak it doesn't matter whether the samples are treated simultaneously or as separate, interleaved groups. The results are identical, and consequently, the systematic sampling errors are identical.*

Method II

Because Method II also acquires the interleaved samples from the four ADCs in four separate memories, equations (64) and (65) apply equally well to Method II. Consequently, the results for the systematic sampling error with the 4 ADCs in Method II are trivially identical to Method I. The same Figures 4, 5, 14, and 15 apply.

CONCLUSION: *Methods I and II deliver identical results for the systematic sampling error. The only exception is the additional noise contributed by the mismatch of dc offsets, gains and bit boundaries among the 4 ADCs used in Method II.*

The Important Conclusions

The extensive analysis in this application note leads to the following significant conclusions:

1) The dominant error in determining the centroid and area of a peak is the random error from ion and gain statistics. This error is inversely proportional to the square root of the number of ions detected in the peak. The best way to reduce this error is to drastically increase the ion collection rates and the number of ions that are counted. This improves mass accuracy, isotope ratio accuracy, and detection limits. Increasing the number of electrons injected into the detector by each ion is beneficial, but of minor impact.

2) The drastically higher ion rates needed for better mass accuracy requires the use of a high-speed digital signal averager to process many ions in the peak from each acceleration pulse. A time-to-digital converter cannot process such high ion rates because of its requirement to detect no more than a single ion in the peak from each acceleration pulse. See ORTEC Application Notes AN57, AN58, and AN59 for further explanations[1, 4, 10].

3) The systematic error resulting from the size of the sampling interval can be readily managed so that it is negligible compared to the random error from ion and gain statistics.

4) Using a single, 500-MS/s ADC with programmed trigger-delay offsets to achieve 2-GS/s sampling (Method I) delivers the same precision and mass accuracy as using four, interlaced, 500-MS/s ADCs (Method II). However Method II is a factor of 3 to 4 more costly, and suffers extra noise because of mismatches in the dc offsets, gains and bit boundaries among the four ADCs. The ORTEC FASTFLIGHT Digital Signal Averager[9] uses Method I.

References

1. ORTEC Application Note AN57, *Dealing with Dead Time Distortion in a Time Digitizer*, (2001).

2. Alan V. Oppenheim and Ronald W. Schafer, *Digital Signal Processing*, Prentice-Hall, Inc., Englewood Cliffs, New Jersey, USA, (1975), pp 26 – 30.

3. William H. Beyer (Ed.), *CRC Standard Mathematical Tables*, 27th Edition, CRC Press, Inc., Boca Raton, Florida, USA, (1984), pp 412 – 421.

4. D. A. Gedcke, ORTEC Application Note AN59, *How Counting Statistics Controls Detection Limits and Peak Precision*, (2001).

5. Ron Jenkins, R. W. Gould, and Dale Gedcke, *Quantitative X-Ray Spectrometry*, Marcel Dekker, New York, First Edition (1981), pp 209 – 229.

6. Phillip R. Bevington, and D. Keith Robinson, *Data Reduction and Error Analysis for the Physical Sciences*, WCB McGraw-Hill, Boston, Second Edition, (1992).

7. *MCP Assembly*, Technical Information, Hamamatsu Application Note, (Sept. 1991), p 7.

8. *Galileo Long-Life Microchannel Plate Brochure*, Burle (formerly Galileo), (1997).

9. U. S. Patent 6,094,627.

10. D. A.Gedcke, ORTEC Application Note AN58, *How Histogramming and Counting Statistics Affect Peak Position Precision*, (2001).

ORTEC®
www.ortec-online.com
Tel. (865) 482-4411 • Fax (865) 483-0396 • info@ortec-online.com
801 South Illinois Ave., Oak Ridge, TN 37831-0895 U.S.A.
For International Office Locations, Visit Our Website

AMETEK®
ADVANCED MEASUREMENT TECHNOLOGY